Ionizational Nonequilibrium Heating During Outer Planetary Entries

Lewis P. Leibowitz* and Ta-Jin Kuo*
Jet Propulsion Laboratory, Pasadena, Calif.

An analytical tool has been developed which enables the impact of ionizational nonequilibrium effects on outer planet entry heating to be estimated. The analysis combines recent shock-tube experiments, flowfield calculations, and planetary entry trajectory analysis. The thickness of the nonequilibrium layer and its variation around the entry body have been correlated by a reaction flow parameter over a wide range of entry conditions. The influence of nonequilibrium effects on heating during entry into Saturn and Jupiter model atmospheres has been studied and the effect of vehicle size and ballistic coefficient determined. An ionizational nonequilibrium layer of significant thickness was found to exist during portions of entry into Saturn and Jupiter warm atmospheres. However, the nonequilibrium layer was found to be thin during the peak heating portions of the trajectory and resulted in reductions in total probe heating of less than 15%.

Introduction

DUE to the timely need for entry-probe design data, recent entry heating studies have neglected the impact of nonequilibrium shock layer flow. However, recent studies by Leibowitz[1] and Howe[2] have indicated that ionizational nonequilibrium effects could result in significant reductions in radiative heating during some outer planet entry missions. The present study includes nonequilibrium entry heating effects and explores their impact on mission design.

The exploration of the outer planets include the study of the structure and composition of the planetary atmospheres. Direct measurements of these properties are possible with the use of an atmospheric entry probe. Heat shield requirements for entry probes under various entry trajectory conditions need to be computed in order to maximize the useful scientific payload and data collection. One assumption that has been consistently applied to the study of outer planet entry heating is that the dissociation and ionization of the hydrogen-helium gas takes place immediately behind the shock wave.[3-10] Thus, the flow in the shock layer is assumed to be in chemical equilibrium.

However, shock-tube measurements of the time history of radiative emission from 8,000-20,000°K hydrogen-helium mixtures have shown that the dissociation and ionization rates are appreciable and for some flowfield conditions may be significantly slow. Also, the radiation emitted by the ionizational nonequilibrium gas behind the shock wave is considerably less than the equilibrium radiative emission. Thus, when the ionization rate is slow compared with the flow rate, a weakly radiating nonequilibrium layer is formed behind the shock wave (see Fig. 1), and the radiative flux impinging on the heat shield is reduced. The assessment of this reduction in heating on heat shield requirements is the main objective of this study.

The ionization kinetics calculation utilizes rate coefficients obtained from shock-tube measurements under simulated entry conditions. Earlier investigations of hydrogen-helium radiative relaxation were performed using dilute mixtures of hydrogen and helium at shock velocities below actual entry velocities, due to shock-tube performance limitations. The recently developed Jet Propulsion Laboratory ANAA shock tube[1] permits conditions which directly simulate outer planetary entry trajectories to be produced. Shock velocities over 50 km/sec into 1.0 torr of hydrogen can be produced which fall well into the range of Jupiter entry conditions. The range of Saturn entry velocities of 25-30 km/sec can be produced over the full range of initial densities encountered during heating. By using radiative relaxation rates obtained with the ANAA shock tube in the ionization kinetics calculations, the uncertainties in predicting nonequilibrium rates have been considerably reduced from previous estimates.

The chemical kinetics calculation has been incorporated into a simplified flowfield computation. The shock layer flowfield was calculated for the spherical nose of an entry vehicle assuming a noncentric shock wave. A correlation expression has been obtained between the nonequilibrium layer thickness and a reaction rate parameter which permits the nonequilibrium calculation to be conveniently combined with a trajectory calculation. The combined nonequilibrium analysis and entry heating program calculate the effect of nonequilibrium reactions on both instantaneous and total entry heating that the heat shield must receive.

Ionization Kinetics and Equations

The reaction scheme describing the important collisional processes in hydrogen-helium ionization relaxation behind shock waves has been modeled after the results of argon ionization studies. Ionization of hydrogen is initiated by atom-atom collisions which produce atoms in electronically excited states that are rapidly ionized by additional collisions. A simplified two-step model is assumed in which hydrogen in the first excited state is produced by collisions with hydrogen and helium atoms and is then immediately ionized by a subsequent collision. As the number of electrons produced by the previous reactions grows, hydorgen is ionized by collisions with electrons. The electron-atom collision process also proceeds by a two-step excitation ionization process, with the first step being the rate controlling reaction.

The reaction scheme for the dissociation of hydrogen has been obtained from results of previous shock-tube investigations.[11,12] Molecular hydrogen is first dissociated by collisions with itself and helium. The hydrogen atoms produced in the reaction also participate in the dissociation reaction, as do ions and electrons as they are formed. In the

Presented as Paper 75-1149 at the AIAA/AGU Conference on the Exploration of the Outer Planets, St. Louis, Mo., Sept. 17-19, 1975; submitted Jan. 14, 1976; revision received April 26, 1976. The work was performed under contract NAS 7-100 of the National Aeronautics and Space Administration. The authors gratefully acknowledge the assistance of A. McRonald in the modification and use of his trajectory program and for his many helpful discussions.

Index categories: Thermochemistry and Chemical Kinetics; Radiation and Radiative Heat Transfer; Supersonic and Hypersonic Flow.

*Member of the Technical Staff, Thermophysics and Fluid Dynamics Section.

lower temperature ranges, when ionization begins to become significant the dissociation rate is fast compared with ionization, and the overall ionization rate is controlled only by the excitation-ionization reactions. However, as the temperature increases, the dissociation time and the ionization time become comparable. At these temperatures, the dissociation rate becomes increasingly important in determining the overall ionization rate.

The rate constants for the reaction scheme have been obtained from the comparison of shock-tube radiation relaxation measurements with the results of computer solutions to the reaction kinetic equations. Radiative relaxation measurements have been made in a 85% hydrogen mixture using the ANAA shock tube. These relaxation time data allow direct comparison of experimental and calculated relaxation times. From a comparison of these results, shown in Fig. 2, expressions for each of the rate constants were obtained and are listed in Table 1. For shock velocities less than 30 km/sec, the dissociation rate was fast compared with the ionization process and thus the overall relaxation rate was controlled by the ionization reaction rates.

In order to calculate nonequilibrium flow around an entry probe, the one-dimensional equations for relaxation rate, fluid mechanics, and equations of state are solved numerically. A different equation is used to describe the rate of formation and destruction of H, H^+, and He^+ by each reaction step in the reaction scheme. The concentrations of the remaining species are obtained using conservation of atomic elements relations. Separate energy equations for electrons and heavy particles are needed to obtain the electron temperature and the heavy particle temperature. A steady-state approximation for the electron energy equation allows an explicit equation of T_e to be written in terms of species concentrations and the heavy particle temperature. For a further description of the governing equations for ionization kinetics, see Leibowitz[11] and Hoffert and Lien.[13]

For one-dimensional, chemically reacting system tube flow, the energy equation and equations of state are solved in terms of the stream tube velocity and pressure, u_2 and p_2, and the species concentrations and the electron temperature. The velocity and pressure are obtained from the shock layer pressure distribution expressions, while the species concentrations are obtained from numerical integration of the kinetic rate equations. A Runge-Kutta integration scheme which starts at the shock wave and follows a streamline through the shock layer is used. The kinetics and fluid relations are solved at each step. A separate step size is used for integration in the dissociation and ionization regions.

Flowfield Computation

Since a large number of serial computations are necessary for computing the nonequilibrium planetary entry shock layer and the radiative flux, none of the time-consuming flowfield computation schemes, such as the method of integral relations, the time-dependent method, or the inverse method is pursued here. Instead, a simplified but rapid flow computation has been developed. A straightforward marching scheme along various streamtubes from the shock front is used, similar to the approaches of Freeman[14] and Hornung.[15] Streamtube calculations of nonequilibrium shock layers have also been performed by Lin and Teare,[16] McKenzie,[17] and Menees.[18] By using several empirical relations from previous exact numerical solutions, the present scheme involves only purely algebraic computation versus the full-fledged boundary-value problem used by the latter two authors. However, the present scheme would be more accurate than Freeman's model, which grossly underestimates the flow speed in regions close to the body and overestimates the thickness. The standoff distance is obtained from the correlation of Hornung[15] in terms of the reaction rate parameter.

It is reasonable to uncouple radiation from the flowfield computation, thus assuming the inviscid shock layer to be

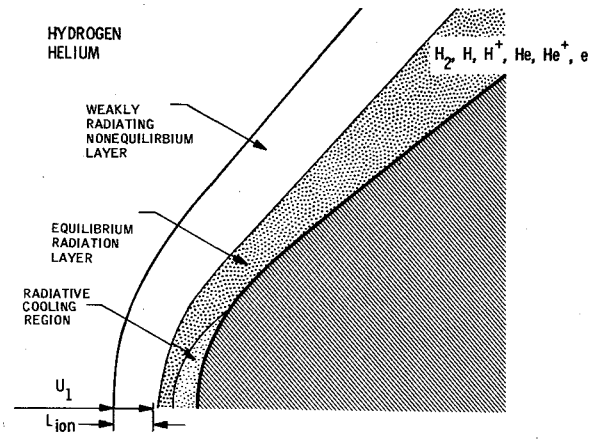

Fig. 1 Schematic diagram of radiative flow regions.

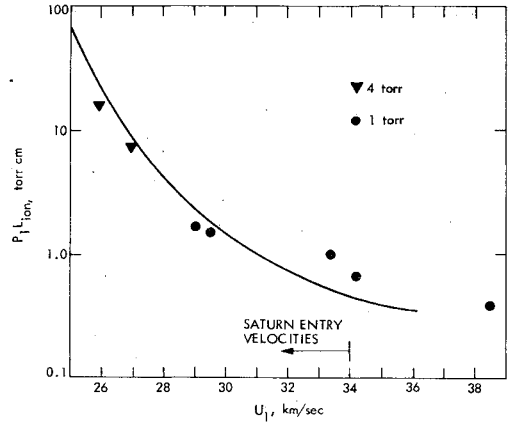

Fig. 2 Comparison of computer calculated values of the normalized ionizational relaxation distance with shock tube measurements, where ● and ▼ represent data using the ANAA shock tube with $p_1 = 1.0$ and 4.0 torr respectively.

radiatively adiabatic for all outer planetary missions except Jupiter. This greatly simplifies the computation of the inviscid shock layer. From our previous computation, the cooling parameter (characteristic radiative flux vs enthalpy convection) is less than 2% throughout the entire flight history for a 0.7 m radius Saturn probe with an inertial entry angle $-\gamma = 40°$, and still less for either a shallower entry or for other outer planets except Jupiter. To simplify calculations, the flowfield around Jovian probes is also computed assuming radiative adiabaticity.

Table 1 Reaction scheme and rate constants

Reactions	Rate constants in $cm^3\ sec^{-1}$
1. $H + e \rightleftharpoons H^+ + 2e$	$k_1 = 6.09 \times 10^{-17} (8kT_e/\pi\mu_e)^{1/2} \exp(-13.6/kT_e)$
2. $He + e \rightleftharpoons He^+ + 2e$	$k_2 = 3.56 \times 10^{-17} (8kT_e/\pi\mu_e)^{1/2} \exp(-24.58/kT_e)$
3. $H + e \rightleftharpoons H^* + e$, $H^* + e \rightleftharpoons H^+ + 2e$	$k_3 = 1.1 \times 10^{-16} (8kT_e/\pi\mu_e)^{1/2} \exp(-10.0/kT_e)$
4. $He + e \rightleftharpoons He^* + e$, $He^* + e \rightleftharpoons He^+ + 2e$	$k_4 = 6.0 \times 10^{-17} (8kT_e/\pi\mu_e)^{1/2} \exp(-20.0/kT_e)$
5. $H + H \rightleftharpoons H^* + H$, $H^* + H \rightleftharpoons H^+ + e + H$	$k_5 = 5.0 \times 10^{-18} (8kT/\pi\mu)^{1/2} \exp(-10.0/kT_o)$
6. $H + He \rightleftharpoons H^* + He$, $H^* + He \rightleftharpoons H^+ + e + He$	$k_6 = 5.0 \times 10^{-18} (8kT/\pi\mu)^{1/2} \exp(-10.0/kT_o)$
7. $H_2 + He \rightleftharpoons H + H + He$	$k_7 = 7.2 \times 10^{-6}\ T \left[1 - \exp(1.5 \times 10^8/T^2)\right] \exp(-52340/T)$
8. $H_2 + H_2 \rightleftharpoons H + H + H_2$	$k_8 = 2.5\ k_7$
9. $H_2 + H \rightleftharpoons H + H + H$	$k_9 = 14.0\ k_7$
10. $H_2 + H^+ \rightleftharpoons H + H + H^+$	$k_{10} = k_9$
11. $H_2 + e \rightleftharpoons H + H + e$	$k_{11} = k_9$

Shock Shape Determination

It is well known that the stand-off distance and the shock shape for a chemically equilibrium inviscid shock layer over a blunt body can be closely approximated by a perfect gas solution with a constant γ that reproduces the compression ratio along the axis. One of the latest investigations along this line with experimental support was described by Miller and Moore.[19] As a corollary, when the stand-off distance for a chemically equilibrium inviscid shock layer is given, the corresponding perfect gas solution that reproduces the stand-off distance will also reproduce the compression ratio and shock shape. As a first approximation, this correlation is extended to shock layers governed by finite-rate kinetics in the present study. In the present scheme, the shock front configuration, as well as those of the streamlines and pressure distribution, are specified prior to the chemical kinetics calculations.

The shock stand-off distance is given by empirical relations extracted from the frozen flow numerical solution of Van Dyke[20] for an infinite Mach number. The numerical discrepancy among the simple empirical relations and Van Dyke's solutions is less than 1.5% in a wide range of compression ratios. However, it should be noted here that with Van Dyke's inverse approach the body configuration is that which supports a paraboloid shock front, and hence is not exactly a sphere. These shock stand-off distance formulas apply equally well to equilibrium flows and are extended here to nonequilibrium studies.

The nonequilibrium stand-off distance is interpolated between the frozen and equilibrium values using Hornung's[15] correlation:

$$\Delta_0 = (\Delta_0)_f - (2+\log\Omega)\ [(\Delta_0)_f - (\Delta_0)_{eq}]/5 \tag{1}$$

The reaction-rate parameter Ω (the first Damköhler number) is defined as the ratio of the fluid mechanic residence time to the reaction time, and for the stagnation point it can be approximated by

$$\Omega = p_1 R_B / u_1 (p_1 t_p) \tag{2}$$

where the normalized particle relaxation time $p_1 t_p$ is obtained from the ionization kinetics calculations.

The shock shape in terms of body-centered coordinates (see Fig. 3) is obtained from the relations between the shock-centered angle and the body-centered angle,

$$\cos\Theta_s = \frac{\sin^2\theta_s}{R_{os}}\left[\delta + \frac{\cos\theta_s}{\sin^2\theta_s}\sqrt{R_{os}^2 - \delta^2\sin^2\theta_s}\right] \tag{3}$$

and the expression for the shock radius,

$$r_s \simeq R_{os}\left[\frac{\sin\Theta_s}{\sin\theta_s} + \frac{\epsilon\,\Theta_s^4}{6\cos(\theta_s - \Theta_s)}\right] \tag{4}$$

where ϵ denotes the ratio of the oncoming flow density to the mean shock layer density along the axis and R_B and R_{os} denote the body radius and the shock radius at the axis, respectively, which are not concentric.

The first term represents the contact sphere at the axis as viewed from the body center. The second term reflects the gradual increase of the radius of curvature of the shock front as it extends from the axis. Due to symmetry requirement, the radius correction term starts with $0(\Theta_s^4)$ as shown.

Pressure Field and the Streamline Configuration

Post-shock pressure along the shock front p_s is computed using frozen-flow oblique shock relations, assuming vibrational equilibrium. Pressure distribution along the axis is given by Bernoulli's equation.

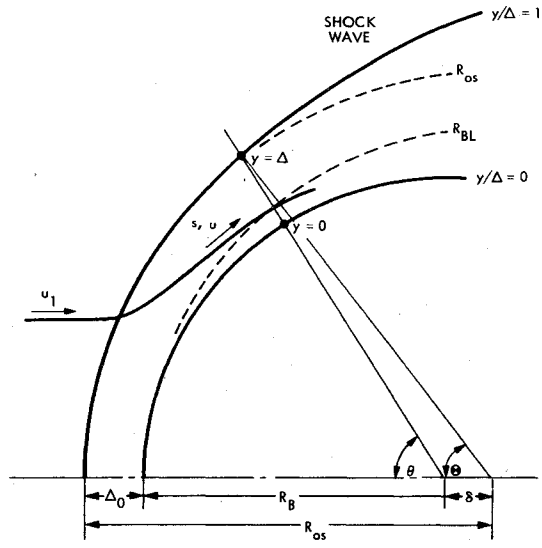

Fig. 3 Schematic diagram of flowfield geometry.

Pressure distribution along the body downstream of the stagnation point is given by the modified Newtonian pressure distribution

$$p_B = p_{B,0}\cos^2\theta = \left(p_{s,0} + \frac{\rho_1 u_1^2}{2}\epsilon\right)\cos^2\theta \tag{5}$$

which is insensitive to the chemistry within the shock layer according to time-dependent solutions of Kyriss.[21] With the pressure fully specified along the boundaries, pressure distribution within the shock layer is approximated by interpolating between $p_B(\theta)$ and $p_s(\theta)$ using the expression:

$$p(\theta, y/\Delta) = p_B + (p_s - p_B)(y/\Delta)^2 \tag{6}$$

which reduces to the correct values at the shock front, at the body, and along the axis.

The streamline configuration is approximated by essentially stretching Lighthill's constant density, concentric shock layer streamlines[22] between the annulus R_{os} and R_{BL} (see Fig. 3) radially in a linear proportion to fill in the $y/\Delta = 1$ and $y/\Delta = 0$ annulus. Thus, at a given θ, the streamline ordinate y/Δ essentially retains its corresponding Lighthill value. The stream function is described by

$$\psi(\theta, r) = \rho_1 u_1 \frac{\left[R_B + \frac{y}{\Delta}\Delta(\theta)\right]^2 \sin^2\theta}{30\,\epsilon_L^2}\left\{3(1-\epsilon_L)^2\bar{r}^4 - 5(1-4\epsilon_L)\bar{r}^2 + 2(1-\epsilon_L)(1-6\epsilon_L)\bar{r}^{-1}\right\} \tag{7}$$

where

$$\bar{r} = \frac{R_B}{R_{os}} + \frac{\Delta_0}{R_{os}}\left(\frac{y}{\Delta}\right)$$

is the stretching parameter and the Lighthill compression ratio ϵ_L, which is different from ϵ, follows from the requirement that the shock and body radii be concentric. Despite the anomalous sonic line configuration of the original Lighthill's solution, the sonic line configuration for a frozen-flow computation with the present scheme agrees closely with much more elaborate schemes. Thus, calculations proceed from the shock front along streamtubes whose configuration and pressure distribution are known. The local flow speed is computed at each station using the Bernoulli's equation with density input from the kinetics computation within the previous

increment. The residence time for the next increment across the flowfield becomes the step size for the kinetics computation. Thus, straightforward stepwise kinetic and flow calculations are carried out along each streamline. For a typical Saturn entry computation, calculations along sixteen streamtubes were carried out to fully cover the flowfield. This flowfield scheme is only meant to be a first-order solution and leaves fine details of iterative schemes to subsequent studies.

Results of Nonequilibrium Calculations

The interaction of ionization processes with the shock layer flowfield can be studied using the ionization kinetic flow calculations. The thickness of the nonequilibrium layer can be determined and the variation of properties along the body obtained. Conditions representative of Saturn entry trajectories have been chosen as examples and the results illustrate the impact of the shock layer flow on the ionization relaxation rate.

Although the three-dimensional flowfield can be broken into one-dimensional streamtubes in order to simplify nonequilibrium calculations, considerable errors are introduced if further simplifications of constant area or constant pressure flow are used. This is due to the difference from streamline to streamline in pressure variation along the streamline. Streamlines in the stagnation region have an increasing pressure, while streamlines away from the stagnation region have a steady decrease in pressure away from the shock wave. The sensitivity of the relaxation rate to streamline pressure distribution limits the accuracy of studies using tabulated constant pressure kinetics calculations for streamline relaxation distances such as recently done by Howe.[2]

Electron Concentration Distribution

The electron concentration and temperature distribution in the flowfield determine the radiative flux to the body. For nonequilibrium flow, the electron concentration and temperature distribution in the flowfield are affected by the reaction time for dissociation and ionization. An example of the electron concentration distribution in the shock layer surrounding a spherical nose is shown in Fig. 4 for initial conditions encountered during a Saturn entry trajectory. The relative thickness of the shock layer has been magnified for illustrative purposes. Lines of constant electron concentration for values of 0.19, 0.39, 0.58, 0.77, and 0.97 of the peak stagnation point electron concentration are shown in terms of y/Δ, the distance from the body normalized by the shock layer separation distance, and the body angle in polar representation. Also shown are the trajectories of two of the streamlines followed in the calculations. The kinetic flow parameter has a value $\Omega = 0.949$ for this case. The region of peak electron concentration is kept close to the body by the long relaxation times, and the peak electron concentrations are confined to the stagnation region due to the decay in electron concentration as the flow expands around the body.

Correlation with Reaction Flow Parameter

In order to achieve a simplified method for including nonequilibrium effects in entry heating calculations, the correlation of shock layer electron distribution with the rate parameter Ω has been studied. Along a trajectory, the entry velocity and initial density vary over a wide range, resulting in changes in shock layer temperature, electron concentration, and Ω. Electron distribution contours for cases with the same Ω have been tested for similarity over the range of conditions of velocity and density encountered during Saturn entry. In Fig. 5, lines of constant electron concentration are plotted as a function of normalized body distance and body angle for three cases having $\Omega = 1.27$. Each case of density and velocity represents an actual point on an entry trajectory (Saturn nominal atmosphere, 40° inertial entry angle) with nose radius adjusted to achieve equal Ω. Electron contours are

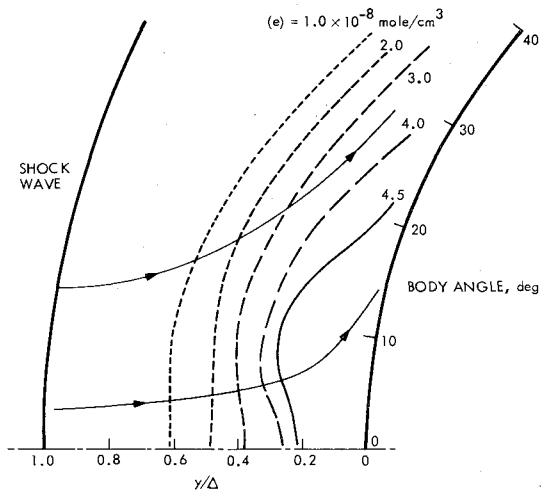

Fig. 4 Nonequilibrium shock layer flow showing lines of constant electron concentration for a Saturn entry case with $R_B = 20$ cm, $u_I = 29.9$ km/sec, $\rho_I = 1.06 \times 10^{-7}$ gm/cm^3, and 40° entry angle, $\Omega = 0.949$.

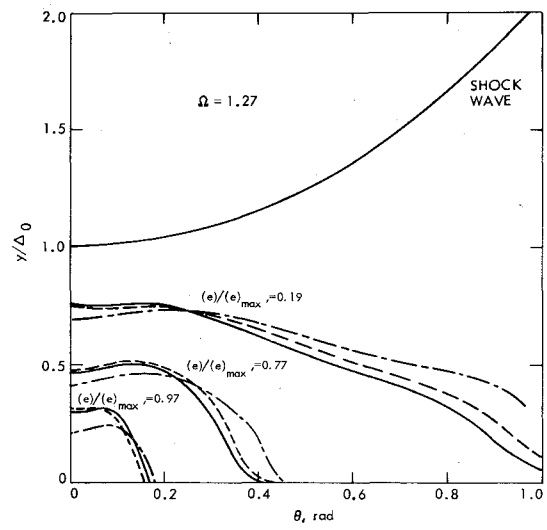

Fig. 5 The use of Ω as a similarity parameter for electron density distribution where the listed parameter is the fraction of maximum electron concentration and the conditions for the calculations are — $\rho_I = 2.69 \times 10^{-7}$ gm/cm^3, u_I27.3 km/sec, $R_B = 70$ cm; --- $\rho_I = 4.36 \times 10^{-7}$ gm/cm^3, $u_I = 28.1$ km/sec, $R_B = 20$ cm; and — — $\rho_I = 1.06 \times 10^{-7}$ gm/cm^3, $u_I = 29.9$ km/sec, $R_B = 27$ cm.

shown in Fig. 5 for values of 0.19, 0.77, and 0.97 of the maximum electron concentration in each case. Despite the significant variation in initial density and nose radii, the contour lines are found to be similar for the most part. Comparisons of electron contour lines have shown similar agreement for cases with values of Ω from 0.95-4.7. Thus, it is possible to develop an approximate representation for the nonequilibrium flowfield around a sphere knowing the equilibrium, stagnation point, electron concentration, and Ω.

For entry heating studies restricted to the stagnation region, additional simplifications can be made in the nonequilibrium flow treatment. A correlation has been obtained between the results of the flowfield calculation for an effective shock layer thickness and the similarity parameter Ω. The effective distance y_e is defined as the distance between the body and the contour line for 0.77 of the maximum electron concentration. This distance is approximately constant for body angles between 0 and 0.25 rad. In Fig. 6 values of y_e/Δ_0 obtained from the flowfield calculations are plotted as a function of Ω. These calculations cover a range of densities from 1.0 to 4.3×10^{-8} gm/cm^3, a range of entry velocities between 2.7 and

Table 2 Model atmosphere composition (1970) by volume

Atmosphere	H_2	He
Saturn cool	0.73	0.263
Saturn nominal	0.886	0.112
Jupiter warm	0.937	0.062
Jupiter nominal	0.865	0.133

2.99×10^6 cm/sec, and a range of nose radii from 20-88 cm. The calculations shown in Fig. 6 are fit well by the simple empirical expression $y_e/\Delta_0 = 0.9\,(1 - e^{-0.5\Omega})$. Also shown in Fig. 6 is a plot of the effective equilibrium layer thickness $y_e/\Delta_0 = 1 - 1/\Omega$, which assumes a constant velocity behind the shock wave. The deviation between this expression and the calculated results is produced by the effect of flow deceleration in the stagnation region on relaxation distance.

Entry Calculations and Results

Nonequilibrium heating calculations of the instantaneous and total heat flux have been made for entry of a probe into Jupiter and Saturn atmospheres. Using the nonequilibrium, stagnation region flow correlation, the radiative relaxation data were combined with radiative flux calculations and a trajectory program to produce entry heating results. Using this approach, the effect of inertial entry angle, vehicle size, ballistic coefficient, and planetary atmosphere on nonequilibrium heating has been determined.

The trajectory program[23] integrates the equation of motion for a probe in inertial, planetocentric coordinates assuming a constant ballistic coefficient and zero lift. The aerodynamic drag force is calculated using the component of planet rotation velocity and probe inertial velocity in the computational plane, at the entry point latitude. Thus, the calculations are correct for equatorial, downwind entry and can be used for nonequatorial entry with small error. Model atmosphere compositions and temperature and density distributions serve as inputs to the calculations. See Table 2 for a listing of atmosphere compositions. At each point in the trajectory the equilibrium shock layer temperature and density are determined using the results of the JPL Thermochemistry Program.[24] Stagnation point convective heat flux is calculated for a nonablating surface using hydrogen-helium thermal conductivity data.

At each point in the trajectory, the reaction flow parameter Ω is calculated based on the instantaneous entry velocity and freestream density. The effective nonequilibrium shock layer thickness is determined from the correlations given by Eq. (1).

The radiative flux to the body for both equilibrium and nonequilibrium layers was calculated using results from the hydrogen-helium flux computations of Stickford.[25] The instantaneous values of nonequilibrium radiative flux, equilibrium radiative flux, and convective heat flux were compiled. These quantities were integrated to give total entry heating.

An example of the radiative heating pulse experienced by a Saturn entry probe is shown in Fig. 7. The instantaneous heat flux is shown as a function of entry time from an altitude of 300 km from the cloud tops. For this case, with 15 deg entry angle and the Saturn cool atmosphere, the effective radiating layer thickness is considerably smaller than the equilibrium layer throughout the entry heating pulse. The maximum value of Ω during the trajectory is 1.7 and occurs close to the point of peak heating. As can be seen in Fig. 7, the presence of the nonequilibrium layer results in an approximately 40% reduction in the peak radiative heating to the stagnation point. Peak convective heating for this case is 5.8 kw/cm^2 and occurs at 18.9 sec.

The relative impact of the nonequilibrium effect on Saturn entry heating is shown in Fig. 8. The reduction in total radiative heating due to nonequilibrium effects and the ratio of equilibrium radiative heating to convective heating is shown as a function of entry angle. Results for both Saturn nominal and cool atmospheres are shown. Nonequilibrium effects produce significant reductions in radiative flux at the lower entry angles with a 50% reduction in flux produced at $-\gamma = 30$ deg inertial for the nominal atmosphere and at $-\gamma = 8$ deg for the cool atmosphere. However, the significance of radiative heating with respect to convective heating increases with entry angle. Due to the higher fraction of helium in the cool atmosphere, shock layer temperatures are higher than for the nominal atmosphere at a given entry velocity. Thus, radiative heating dominates heating for large angle entry into the cool atmosphere. As a result of the opposite trends in the quantities shown in Fig. 8, the overall impact of the

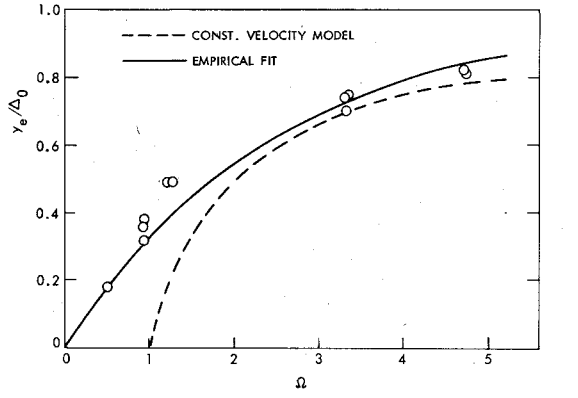

Fig. 6 Correlation of effective equilibrium layer thickness with Ω where o represents results of the flowfield computations: —— denotes an empirical fit to these results, and ----- represents the expression $y_e/\Delta_0 = 1 - 1/\Omega$.

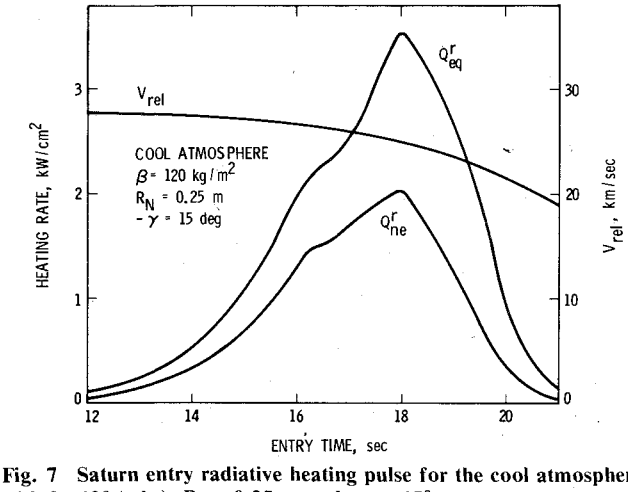

Fig. 7 Saturn entry radiative heating pulse for the cool atmosphere with $\beta = 120$ (mks), $R_N = 0.25$ m, and $-\gamma = 15°$.

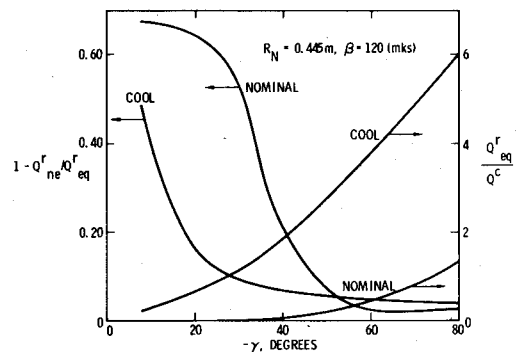

Fig. 8 The reduction in radiative heating due to nonequilibrium effects for Saturn entry with $R_N = 0.445$ m and $\beta = 120$ (mks).

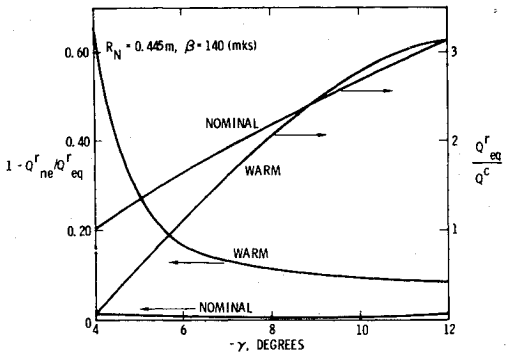

Fig. 9 The reduction in radiative heating due to nonequilibrium effects for Jupiter entry with $R_N = 0.445$ m and $\beta = 140$ (mks).

nonequilibrium effect on the total probe heating is small. Reductions in total heating have been found to be less than 15%.

The effects of radiative relaxation on entry heating for Jupiter nominal and warm atmospheres are shown in Fig. 9. Negligible reduction in radiative heating was found for the nominal atmosphere. Due to lower shock layer temperatures, reductions in heating were apparent for the warm atmosphere. However, even for the warm atmosphere the nonequilibrium effect produces less than a 10% reduction in total entry heating.

Conclusions

An analytical tool has been developed which enables the impact of the ionizational nonequilibrium effect on outer planet entry heating to be estimated. A calculation method was developed to obtain nonequilibrium electron concentration and temperature distributions in an entry probe shock layer based on recent shock-tube radiative relaxation measurements. The thickness of the nonequilibrium layer and its variation around the entry body have been correlated by the reaction flow parameter Ω over a wide variety of entry conditions and nose radii. Using such a correlation in conjunction with entry trajectory calculations, the stagnation region nonequilibrium heating has been studied. The influence of inertial entry angle, vehicle size, ballistic coefficient, and planetary atmosphere has been determined.

An ionizational nonequilibrium layer of significant thickness has been found to exist during entry of a planetary probe into the atmospheres of Saturn and into the warm atmosphere of Jupiter. This nonequilibrium layer forms immediately behind the shock wave and produces appreciably less radiative flux than if in equilibrium. Although the thickness of this zone of low radiation can be an appreciable fraction of the shock layer during the early stages of entry, it was found to be thin during the peak heating portion of the trajectory. Therefore, for the cases considered, ionizational nonequilibrium effects result in only a small reduction in the overall entry heating. Typical reductions are less than 15%.

Consideration of ionizational nonequilibrium effects on outer planet entry missions is still required. Potential changes in probe design or in estimate of planetary atmosphere composition may alter the significance of the nonequilibrium effect on heating. Efforts to reduce probe radiative heating by reducing the nose radius or the ballistic coefficient, for example, will increase the presence of a nonequilibrium layer. Also, nonequilibrium effects may have an impact on other aspects of entry. For example, they must be evaluated if experiments are proposed to monitor shock layer radiative emissions during entry. Finally, further work is required to evaluate nonequilibrium effects on entry into Uranus or other outer planet targets.

References

[1] Leibowitz, L. P., "Jupiter Entry Simulation with the ANAA Shock Tube," AIAA Paper 74-610, Bethesda, Md., 1974.

[2] Howe, J. T., "Hydrogen Ionization in the Shock Layer for Entry into the Outer Planets," *AIAA Journal*, Vol. 12, June 1974, pp. 875-876.

[3] Stickford, G. H. and Menard, W. A., "Bow Shock Composition and Radiation Intensity Calculations for a Ballistic Entry Into the Jovian Atmosphere," AIAA Paper 68-787, Los Angeles, Calif., 1968.

[4] Tauber, M. E. and Wakefield, R., "Heating Environment and Protection During Jupiter Entry," AIAA Paper 70-1324, Houston, Texas, 1970.

[5] Tauber, M. E., "Heat Protection for Atmospheric Entry into Saturn, Uranus, and Neptune," *Advances in the Astronautical Sciences*, Vol. 29, Part II, 1971, pp. 215-228.

[6] Page, W. A., "Aerodynamic Heating for Probe Vehicles Entering the Outer Planets," *Advances in the Astronautical Sciences*, Vol. 29, Part II, 1971, pp. 191-214.

[7] Wilson, K. H., Woodward, H., Tauber, M. E., and Page, W. A., "Jupiter Probe Heating Rates," unpublished paper presented at the Symposium on Hypervelocity Radiating Flow Fields for Planetary Entry, Jet Propulsion Laboratory, Pasadena, Calif., 1972.

[8] Nicolet, W. E., Morse, H. L., and Vojvodich, N. S., "Outer Planet Probe Entry Thermal Protection: Part I: Aerothermodynamic Environment," AIAA Paper 74-700, Boston, Mass., 1974.

[9] Nicolet, W. E., Howe, J. T., and Mezines, S. A., "Outer Planet Probe Entry Thermal Protection: Part II: Heat Shield Requirements," AIAA Paper 74-701, Boston, Mass., 1974.

[10] Sutton, K., "Radiative Heating About Outer Planet Entry Probes," AIAA Paper 75-183, Pasadena, Calif., 1975.

[11] Leibowitz, L. P., "Measurements of the Structure of an Ionizing Shock Wave in a Hydrogen-Helium Mixture," *Physics of Fluids*, Vol. 16, 1973, pp. 59-68.

[12] Leibowitz, L. P., Menard, W. A., and Stickford, G. H., "Radiative Relaxation Behind Strong Shock Waves in Hydrogen-Helium Mixtures," *Proceedings Ninth International Shock Tube Symposium*, Stanford University Press, 1973, pp. 306-317.

[13] Hoffert, M. and Lien, H., "Quasi-One-Dimensional Gas Dynamics of Partially Ionized Two-Temperature Argon," *Physics of Fluids*, Vol. 10, 1967, pp. 1769-1777.

[14] Freeman, N. C., "Non-equilibrium Flow of an Ideal Dissociating Gas," *Journal of Fluid Mechanics*, Vol. 4, 1958, pp. 407-425.

[15] Hornung, H. G., "Non-equilibrium Dissociating Nitrogen Flow Over Spheres and Circular Cylinders," *Journal of Fluid Mechanics*, Vol. 53, 1972, pp. 149-176.

[16] Lin, S. C. and Teare, J. D., "A Streamtube Approximation for Calculation of Reaction Rates in the Inviscid Flow Field of Hypersonic Objects," *Proceedings of the Sixth Symposium on Ballistic Missile and Aerospace Technology: Reentry*, Vol. 4, Academic Press, New York, 1961, p. 35.

[17] McKenzie, R. L., "A Correspondence of Blunt-Body Non-Equilibrium Shock Layers," *AIAA Journal*, Vol. 6, May 1968, pp. 944-946.

[18] Menees, G. P., "A Method for Computing the Non-equilibrium Radiant Emission from Near-equilibrium Shock Layers," *AIAA Journal*, Vol. 9, Feb. 1971, pp. 351-352.

[19] Miller, C. G. and Moore, J. A., "Shock Shapes of Blunt Bodies in Hypersonic Helium, Air, and CO_2 Flows," *AIAA Journal*, Vol. 12, March 1974, pp. 411-413.

[20] Hayes, W. D. and Probstein, R. F., *Hypersonic Flow Theory*, 2nd ed., Academic Press, New York, 1966, pp. 420 and 463.

[21] Kyriss, C. L., "A Time Dependent Solution for the Blunt Body Flow of a Chemically Reacting Gas Mixture," AIAA Paper 70-771, Los Angeles, Calif., 1970.

[22] Lighthill, M. J., "Dynamics of a Dissociating Gas, Part I, Equilibrium Flow," *Journal of Fluid Mechanics*, Vol. 2, 1957, p. 1.

[23] McRonald, A. D., private communication, Jet Propulsion Laboratory, Pasadena, Calif.

[24] Horton, T. E. and Menard, W. A., "A Program for Computing Shock Tube Gasdynamic Properties," Jet Propulsion Laboratory, Pasadena, Calif., TR32-1350, 1969.

[25] Stickford, G. H., "Total Radiative Intensity Calculations for 100% H_2 and 87% H_2-13% He," *Journal of Quantitative Spectroscopic Radiation Transfer*, Vol. 12, 1972, pp. 525-529.